Comparison of structural, magnetic and electrical transport behavior in bulk and nanocrystalline Nd-lacunar Nd0.67Sr0.33MnO3 manganites

Article *in* Journal of Magnetism and Magnetic Materials · February 2019

DOI: 10.1016/j.jmmm.2018.09.124

Arun Bahuleyan Nair
National Institute for Interdisciplinary Science and Technology

Vijay R. Akshay
National Institute for Interdisciplinary Science and Technology

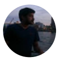

Kakarla Devi Chandrasekhar
National Sun Yat-sen University

Geeta Rani Mutta
Heriot-Watt University

Journal of Magnetism and Magnetic Materials 472 (2019) 74–85

Contents lists available at ScienceDirect

Journal of Magnetism and Magnetic Materials

journal homepage: www.elsevier.com/locate/jmmm

Research articles

Comparison of structural, magnetic and electrical transport behavior in bulk and nanocrystalline Nd-lacunar $Nd_{0.67}Sr_{0.33}MnO_3$ manganites

B. Arun[a,b], V.R. Akshay[a,b], K. Devi Chandrasekhar[c], Geeta R. Mutta[d], M. Vasundhara[b,*]

[a] Materials Science and Technology Division, CSIR-National Institute for Interdisciplinary Science and Technology, Trivandrum 695 019, India
[b] Academy of Scientific and Innovative Research, CSIR- National Institute for Interdisciplinary Science and Technology, Trivandrum, India
[c] Department of Physics, National Sun Yat-Sen University, Taiwan
[d] Heriot-Watt University, Edinburgh EH14 4AS, United Kingdom

ABSTRACT

Bulk and nanocrystalline Nd-lacunar $Nd_{0.67}Sr_{0.33}MnO_3$ manganites were synthesized, and the structural, magnetic and electrical properties have been systematically studied. The Rietveld refinement confirms perovskite structure with orthorhombic crystal symmetry (Pbnm space group). The bulk compound shows a sharp second order transition at 275 K while the nanocrystalline compound exhibit a broadened transition with a T_C of 242 K. Temperature dependence of electrical resistivity of both the compounds witness double peaks; a sharp peak near T_C and a broad peak below $T_{C,}$ which is more prominent in the nanocrystalline compound whereas former peak is more prominent in the bulk compound. The combined effect of Kondo-like spin-dependent scattering and electron-electron interactions dominates the transport properties at low temperature in the nanocrystalline compound and results in upturn enhancement in resistivity, while the high-temperature insulating behavior of both compounds can be explained by the adiabatic small polaron hopping mechanism. The effective Mn ion valence of bulk and nanocrystalline compounds are found to be 3.56 and 3.25 and the observed crystal field splitting energy is slightly higher for the nanocrystalline compound. X-ray absorption spectra result quantitatively demonstrates that the broken symmetry at the surface of nanocrystalline compound aid to stabilize more Mn^{3+} ions that lead to interesting magnetic and electrical transport behavior.

1. Introduction

Perovskite manganites of $A_{1-x}A'_xMnO_3$ (A = rare earth ion, A′ = divalent alkaline earth ion) have drawn wide attention because of their interesting physical phenomena such as colossal magnetoresistance (CMR) and magnetocaloric effect (MCE) etc. [1–3]. The structure, magnetic and electrical properties of these materials are strongly correlated due to the competing interplay between charge, spin and orbital ordering [4–7]. Thus, any changes in the valency at the A-site significantly affects the ferromagnetism and conduction and has been explained on the basis of double exchange (DE) mechanism with a strong on-site Hund's coupling [8]. However, it is understood that the properties of perovskite manganites can also be affected by strong electron-phonon interaction due to the Jahn-Teller distortion, cationic size mismatch, oxygen deficiency and charge ordering [9–16]. In mixed valence manganites, solid solutions with x = 0.33 is an interesting composition which exhibits ferromagnetism and conductivity and shows the most prominent value of Curie temperature [17–22].

Recent studies show that the structure and properties of manganites are severely influenced by the introduction of deficiency at the A-site, and it leads to competing magnetic phases due to the enhancement of disorder effect [23–31]. Again, the introduction of vacancy at the A-site of $A_{0.67}A'_{0.33}MnO_3$ composition is an interesting study because one can further tune the magnetic properties and transition temperature (T_C). However, most of the investigations are reported on bulk materials, and only limited studies are available about the same in the nanocrystalline materials. The conventional solid-state method is the most widely used technique for the preparation of polycrystalline bulk materials, which needs high sintering temperatures because the starting reagents such as oxides and carbonates do not react with each other at ambient temperatures. Here, thermodynamics and kinetics are the two precious parameters to be considered because the former determines the possibility of a reaction, while the later control the chemical reaction rate. Due to the high sintering temperature and long annealing time a desired polycrystalline material of homogeneous composition is obtained. However, sol-gel is a low-temperature solution-based chemical method adopted as a promising technique for synthesizing nanocrystalline materials. It has a precious control over particle size, morphology, homogeneity and phase formation than other traditional techniques [32]. The sol-gel method involves a two-step process. The first step is the chelation between cations and citric acid while the second step is the polyesterification process by hydroxycarboxylic acid with ethylene glycol [33]. The obtained viscous gel was dried and annealed at low-temperature to control the particle size, stoichiometry and makes it an

* Corresponding author.
E-mail address: mvas@niist.res.in (M. Vasundhara).

https://doi.org/10.1016/j.jmmm.2018.09.124
Received 19 July 2018; Received in revised form 14 September 2018; Accepted 30 September 2018
Available online 02 October 2018

excellent method for synthesizing high purity nanocrystalline materials for functional applications. Manganites are not only ascribed in the context of strongly correlated electron systems but also its possibility in modulating their physical and chemical properties at the nanoscale which may be of great interest from the technological point of view [34–39]. Recently, our group has reported a comparative study between bulk and nanocrystalline $Nd_{0.67}Sr_{0.33}MnO_3$ and found that the magnetic ordering and electrical transport properties are strongly governed by the crystalline nature of the compound [40]. As a continuing effort, in the present investigation, we introduced a deficiency of x = 0.17 at the Nd-site of both bulk and nanocrystalline $Nd_{0.67-x}\square_xSr_{0.33}MnO_3$ (i.e., $Nd_{0.50}\square_{0.17}Sr_{0.33}MnO_3$) compounds and investigated the effects on structural, magnetic and electrical transport properties.

2. Experimental

The bulk and nanocrystalline compounds were prepared using solid state and sol-gel technique respectively. The preparation methods were reported in our previous works [40,41]. The crystal structure was characterized by X-ray diffraction (XRD) analysis using Ni-filtered Cu Kα radiation (PANalytical X'Pert Pro Diffractometer), and the Rietveld refinement was performed using the FullProf software. The Iodometric titration method was performed to estimate the Mn^{3+}/Mn^{4+} ratio and the oxygen stoichiometry [42,43]. Powders were weighed and dissolved in a mixture of 10 ml of 10 mass % potassium iodide aqueous solution and 2.5 ml of 2 M hydrochloric acid. The iodine liberated in the reaction was titrated against 0.1 N sodium thiosulphate standard volumetric solution, and starch solution (1 mass %) was used as an indicator. Under the assumption that Mn is in a mixed state of Mn^{3+}/Mn^{4+}, the chemical formula of both bulk and nanocrystalline compounds can be written as $Nd^{3+}_{0.67-x}Sr^{2+}_{0.33}Mn^{3+}_{1-\alpha}Mn^{4+}_{\alpha}O_y$ (x = 0.17). The value of α was determined by the iodometric titration method, and the average ratio of Mn^{3+}/Mn^{4+} was calculated for 5 titrations [42,43]. The morphological analysis of bulk and nanocrystalline compounds were investigated by scanning electron microscopy (SEM) and transmission electron microscopy (TEM) respectively. The stoichiometry of the compounds was confirmed by X-ray Fluorescence Spectrometry (EDXRF) analysis (PANalytical Epsilon 3). X-ray absorption spectra (XAS) was performed using total electron yield mode under chamber base pressure of $\sim 10^{-9}$ Torr (National Synchrotron Radiation Research facility, Taiwan). Magnetic properties and electrical resistivity were measured using vibrating sample magnetometer and electrical transport option attached to the physical property measurement system (Quantum Design Inc., USA).

3. Results and discussion

The XRD patterns of both bulk and nanocrystalline compounds confirm that it belongs to orthorhombic symmetry with Pbnm space group. The Rietveld refinement of XRD patterns is shown in Fig. 1 and refined structural parameters obtained are listed in Table 1. The weighted pattern $R_{WP,}$ pattern R_P and goodness of fit χ^2 show small values indicating good agreement between the calculated and observed XRD data. In the bulk compound, we have found an additional peak around 36° indicates the presence of minor secondary phase (rhombohedral ferrimagnetic Mn_3O_4 phase). It has been reported that the formation of Mn_3O_4 phase is due to the preparation method, essentially the manual grinding step which sometimes does not ensure a perfect homogeneity [44]. However, it has been also reported that cation vacancy leads to the formation of Mn_3O_4 [45]. It is to be noted that nanocrystalline compound didn't show any kind of such impurity phases in the XRD plot. The average crystallite size is calculated from the XRD peaks using Scherer's formula [46] as

$$D= K\lambda/\beta\cos\theta \quad (1)$$

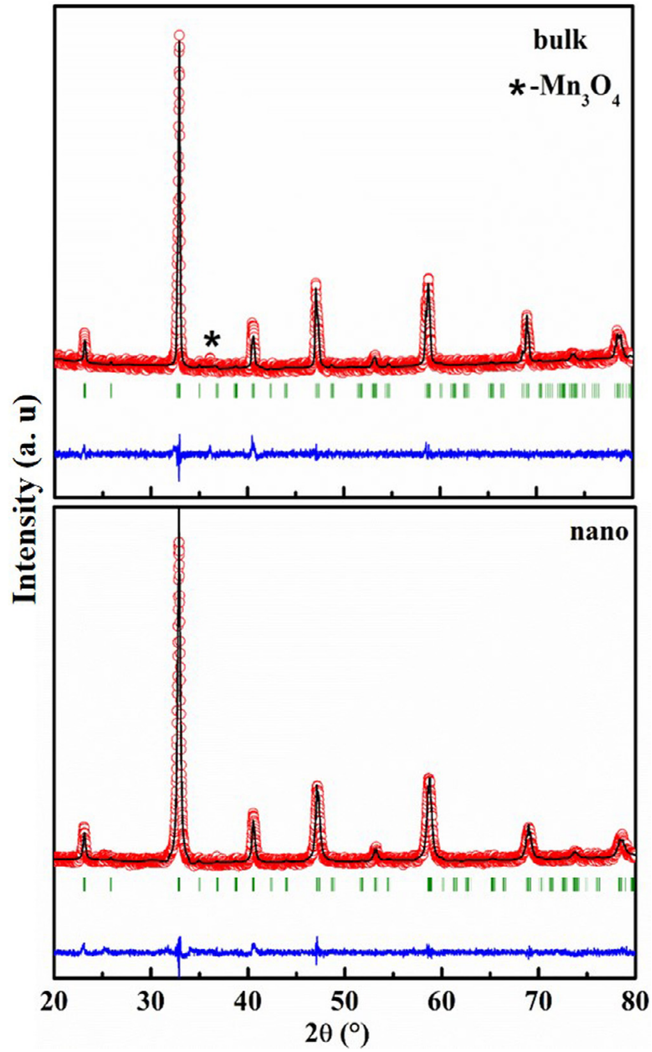

Fig. 1. Refined XRD patterns of bulk and nanocrystalline $Nd_{0.50}\square_{0.17}Sr_{0.33}MnO_3$ compounds. The bottom (blue) line represents the difference between the XRD data (red) and calculated fit (black) and the green lines are Bragg positions. (For interpretation of the references to colour in this figure legend, the reader is referred to the web version of this article.)

where K is the shape factor lying between 0.9 and 1.15, λ is the wavelength of X-ray, β is the corrected full-width half maxima of the XRD peaks and θ is the Bragg angle. The crystallite sizes are found to be in the range of 33 nm (± 8 nm) for bulk compound and 19 nm (± 4 nm) nm for the nanocrystalline compound. The theoretical density was calculated from the refinement analysis as 5.471 g/cm^3 and 5.462 g/cm^3 for bulk and nano compounds respectively. The density of the sintered pellets was measured by using the Archimedes method and both compounds exhibit above 95% densification. The introduction of vacancy at the Nd-site will reduce the average A-site cationic radius and result in the reduction of lattice parameter and unit cell volume, which further affects DE interaction between Mn^{3+} and Mn^{4+}. The ratio of Mn^{3+} and Mn^{4+} content in $Nd_{0.67-x}\square_xSr_{0.33}MnO_3$ compound are (0.67 − 3x) and (0.33 + 3x) respectively. The Nd-deficiency increases the number of Mn^{4+} content and a corresponding reduction in the number of Mn^{3+} ions, which in turn leads to the contraction of the unit cell volume, which is in agreement with earlier reports about the La/Pr deficient manganites [31,44,47]. But, in the case of strontium deficient manganites, an increase in the unit cell volume is noticed with increase of Sr-deficient content [26,31,48]. Further, it is well reported that Nd/La/Pr -deficiency and Sr/Ca/Ba/Na-deficiency have an inverse effect on the unit cell volume of the stoichiometric compounds

Table 1
Refined structural parameters obtained from the Rietveld analysis.

	Bulk	Nanocrystalline
Cell parameters		
a (Å)	5.4679	5.4590
b (Å)	5.4367	5.4491
c (Å)	7.6743	7.6798
V (Å^3)	228.21	228.45
Positional parameters		
Nd/Sr x	0.5003	0.4970
Nd/Sr y	0.0181	0.0156
O1 x	0.5612	0.5443
O1 y	0.4988	0.5132
O2 x	0.2133	0.1912
O2 y	0.2868	0.2935
O2 z	0.0258	0.0308
Bond distance (Å)		
$< d_{Mn\text{-}O} >$	1.953(2)	1.959(2)
Bond angle (°)		
Mn-O1-Mn	159.652(6)	153.152(6)
Mn-O2-Mn	160.199(3)	165.023(1)
Agreement factors		
R_{WP}	4.03	2.95
R_P	3.14	2.29
χ^2	1.4	1.7

[24,26–28,31,44,47–49]. Hence, in order to further elucidate the Mn^{3+}/Mn^{4+} ratio, we have carried out the iodometric titration method and found that the ratio of Mn^{3+}/Mn^{4+} to be 1.13 and 1.44 with an accuracy of ± 0.02 for bulk and nanocrystalline Nd-deficient compounds respectively. It is to be noted that the ratio of Mn^{3+}/Mn^{4+} was found to be 2.03 for the stoichiometric compound ($Nd_{0.67}Sr_{0.33}MnO_3$) reported earlier [40]. Thus the iodometric titration method quantitatively demonstrates that both bulk and nanocrystalline Nd-deficient compound contains more Mn^{4+} ions than that of its stoichiometric compound. Since the average ionic radius of Mn^{4+} (0.53 Å) is less than that of Mn^{3+} (0.645 Å), the cell volume of both the bulk and nanocrystalline Nd-deficient compounds show lesser values than that of its stoichiometric compound [40]. The amount of oxygen content, y, was estimated from the iodometric titration using the equation as [42,43]

$$y = 3 \pm \delta = \frac{17 + 3\alpha}{6} - x \tag{2}$$

The oxygen stoichiometry is found to be 2.90 and 2.87 for the bulk and nanocrystalline compounds respectively. Since the nanocrystalline compound contains more oxygen deficiency, the average oxidation state of Mn-ions is expected to decrease and thereby increases the average Mn-ionic radius results in a corresponding increase in the unit cell volume [50]. Since it is observed that the nanocrystalline Nd-deficient compound contains more Mn^{3+} ions than that of the bulk Nd-deficient compound, the former shows greater cell volume (228.45 Å^3) than that of the later (228.21 Å^3). Thus, the change in the lattice parameters and unit cell volume of the bulk and nanocrystalline compounds can be attributed due to the combined effect of the difference in the ionic radius between Mn^{3+}/Mn^{4+} and the presence of vacancies at the oxygen sites. Moreover, the oxygen vacancies in the Mn-O-Mn network affects the tolerance factor due to lattice distortion, which in turn affects the Mn—O bond lengths and Mn—O—Mn bond angles [50]. Thus the electron hopping between Mn^{3+}/Mn^{4+} ions are strong influences by the lacunar at the A-sites and oxygen deficiency.

Fig. 2(a) and (b) represent the SEM images of highly densified bulk and nanocrystalline compounds with homogeneous surface. Micrometre size grains with grain boundaries are seen in the SEM image of the bulk compound. However, the nanocrystalline compound was taken at 200 nm scale which confirms the nanocrystalline nature of the compound. Fig. 2(c) and (d) represent the TEM image of bulk and nanocrystalline compounds taken at 100 nm and 50 nm scale respectively. In case of the bulk compound, the size determined from the TEM analysis is found to be greater than that of using Scherer's formula. This discrepancy in size may be due to the fact that the single particle may consist of more than one crystallite. The TEM image of nanocrystalline compound reveals particle size of 25–30 nm. This value is close to those obtained for the crystallite size by using Scherer's formula. Fig. 2(e) and (f) represent the EDAX spectrum of bulk and nanocrystalline compounds. The selected area electron diffraction pattern (SAED) is shown in the inset, which confirms the high crystalline nature of the compounds and planes are identified and corroborates with that of its XRD patterns. The energy dispersive X-ray spectroscopic analysis (EDAX) confirm the stoichiometry and homogeneity of the compounds. We have performed EDXRF analysis to determine the Nd – deficiency and the stoichiometric composition of both bulk and nanocrystalline compounds. The percentage of elemental oxides observed during the EDXRF analysis are given in Table 2. It is clear from the table that the stoichiometric ratio between Nd and Sr are maintained for bulk (0.491: 0.33 with a vacancy □ = 0.179), and nanocrystalline (0.498: 0.33 with a vacancy □ = 0.172) compounds within the limits of experimental error.

The influence of nanosize effects on the electronic structure and valence states of manganese and oxygen ions have been verified with the XAS. Fig. 3(a) represents the normalized XAS spectra recorded at 300 K near L-edge of Mn and K-edge of O for both compounds. The spectra of Mn^{2+}, Mn^{3+} and Mn^{4+} are plotted in the same figure for the comparison purpose, and shifted vertically for clarity. Both the compounds showed two broad L_{III} and L_{II} peaks of Mn 2p owing to the spin-orbit coupling [51]. Bulk compound peaks (L_{III} and L_{II}) show pronounced shoulder (marked by an arrow) with well-defined maxima. However, the nanocrystalline compound exhibits a noticeable change in the shape compared to the bulk compound. Both L_{III} and L_{II} peaks of the nanocrystalline compound are much broader than its bulk counterpart with hump-like features noticed (shown as arrows in Fig. 3(a)) on lower energy sides of both L_{III} and L_{II} peaks. Both the compounds show spectra features resemble to superimpose of both Mn^{3+} and Mn^{4+}. The maximum of L_{III} peak falls between Mn^{3+} and Mn^{4+} in accordance with the previous reports on the CMR manganites [52]. But, in the case of the nanocrystalline compound, the peak positions of L_{III} and L_{II} shifted towards the lower energy side in comparison to that of the bulk one. The change in the effective valence state of Mn-ions results in a chemical shift in the L_{III} and L_{II} peaks and variation in the symmetry of the ground state changes the spectral shape of the compounds [51]. Using the interpolation method, we have calculated the effective oxidation state of Mn-ions and depicted in Fig. 3(b). As shown in the figure, the photo energy versus Mn valence exhibit linear variation. The interpolated average Mn valence from the peak position indicates 3.56 and 3.25 valence states for bulk and nanocrystalline compounds respectively. This result quantitatively demonstrates that the Mn^{3+} ions increases in case of the nanocrystalline compound in compared to its bulk counterparts. This is because of the broken symmetry at the surface of nanoparticles aid to stabilize more Mn^{3+} ions in the nanocrystalline compound. Fig. 3(c) shows the oxygen 1s XAS for both the compounds. The characteristic peaks of oxygen K-edge are used to identify the hybridization between the transition metal ions to the ligand ions, and the spectrum of O K-edge can be split into three types. First and second peaks assigned to the excitation of O 1 s state to O2p-Mn3d (~528 eV) and O2p-Nd5d (~536 eV) states respectively. The third peak attribute to the excitation of O 1s state to O2p-Mn4sp state (~543 eV) [53,54]. The octahedral crystal field splitting of e_g and t_{2g} symmetries can be seen from the peaks separation in the shaded area, and the intensity of peak is proportional to the number of unoccupied hybridized density of O2p-Mn3d states [54]. From Fig. 3(c), it is clear that the first peak intensities of nanocrystalline compound are much lower and that signifies the less number of hole doping appeared in the compound. On the other hand, the observed crystal field splitting energy is slightly higher for the nanocrystalline compound, which could

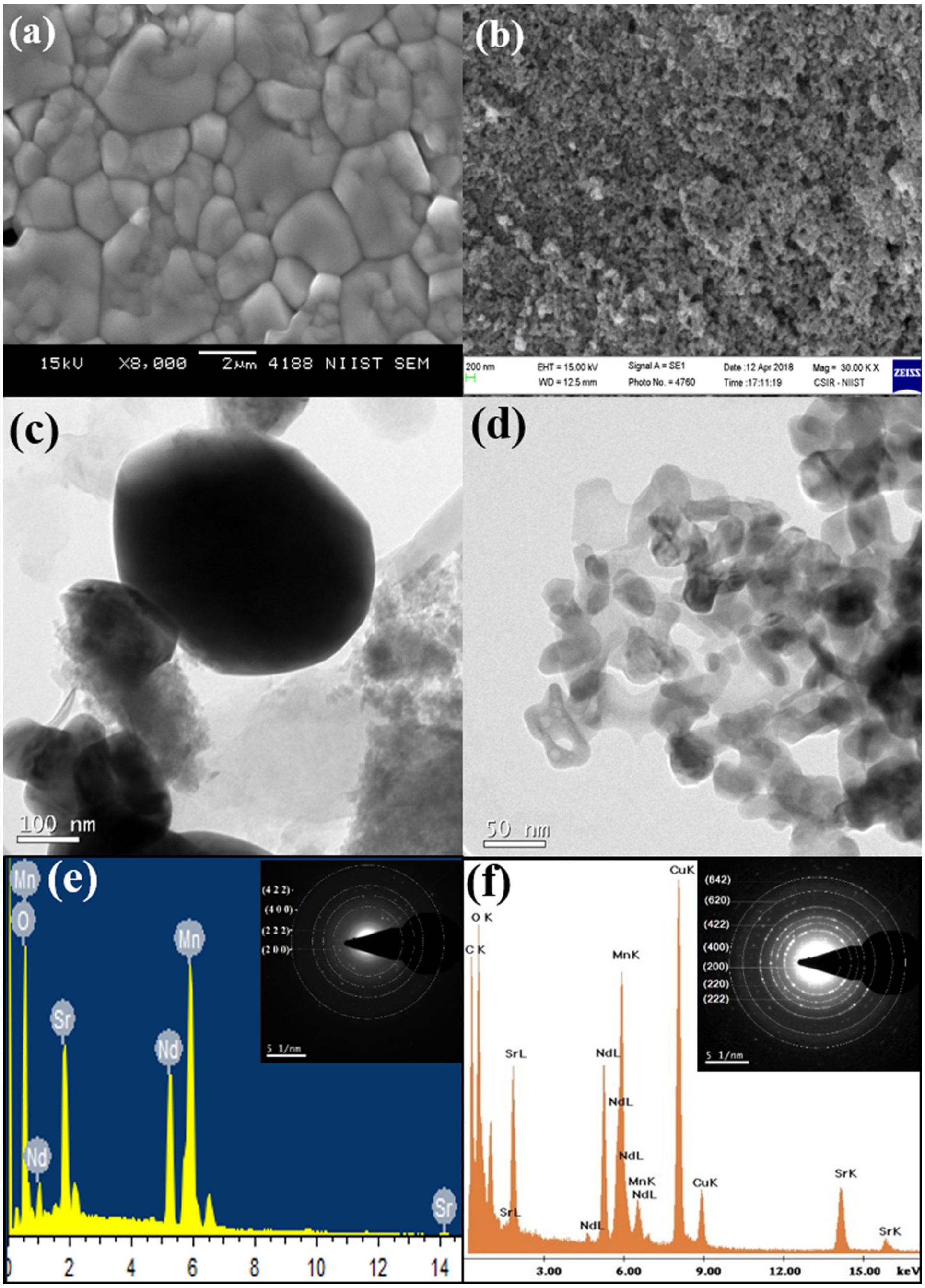

Fig. 2. (a) and (b) SEM images, (c) and (d) TEM images, (e) and (f) EDAX spectrum of bulk and nanocrystalline $Nd_{0.50}\square_{0.17}Sr_{0.33}MnO_3$ compounds respectively. SAED patterns are shown in the inset.

Table 2
Percentage of element oxide obtained from the EDXRF analysis.

Element oxide	Bulk	Nanocrystalline
Nd_2O_3	44.649	49.371
SrO	18.510	20.129
MnO	36.841	30.500

be assigned to the presence of more Mn^{3+} ions that lead to large field splitting.

Temperature variation of magnetization, M (T), has been carried from 2 K to 300 K under 50 Oe and is depicted in Fig. 4. There is strong thermo-magnetic irreversibility is seen in between the zero-field-cooled (ZFC) and field cooled (FC) curves due to the magnetic frustration in the compounds [55]. Also, it can be seen that bulk compound show a hump like character around 46 K and it is due to the ordering of Mn_3O_4 present in the compound. However, we did not observe any kind of such low-temperature transition in the case nanocrystalline compound. The T_C is calculated from the derivative of magnetization (dM/dT) versus temperature, and the bulk compound shows a sharp transition with a T_C of 275 K and nanocrystalline compound exhibit a broadened transition with a T_C of 242 K. However, it can be seen that both bulk and nanocrystalline compounds show higher T_C than its stoichiometric compound $Nd_{0.67}Sr_{0.33}MnO_3$ [40], and it may be due to the increase in DE interaction with the creation of lacuna at the Nd-site. However, from the Fig. 4, it can be seen that the nanocrystalline compound shows a crossover in FC magnetization curve around 134 K, below which magnetization values are higher for nanocrystalline compound. This

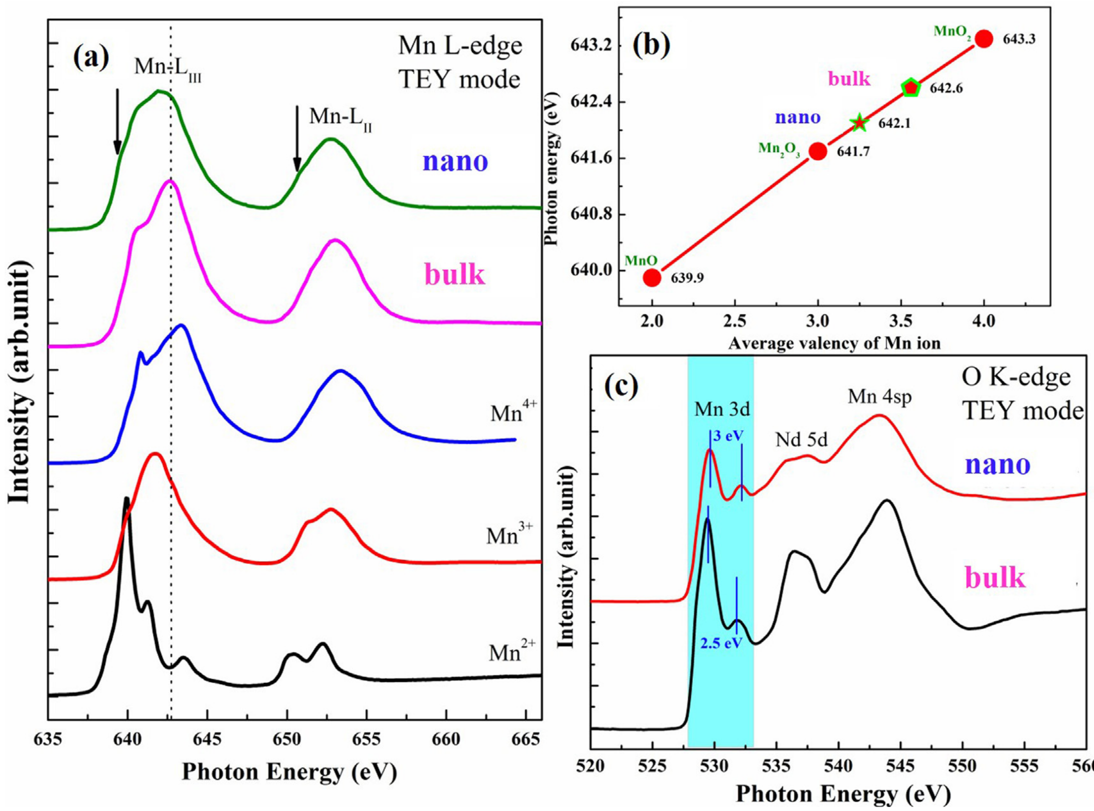

Fig 3. X-ray absorption spectroscopic images of bulk and nanocrystalline $Nd_{0.50}\square_{0.17}Sr_{0.33}MnO_3$ compounds. (a) Mn 2p XAS for both the compounds; (b) photo energy versus Mn valence for both the compounds; (c) oxygen 1s XAS for both the compounds.

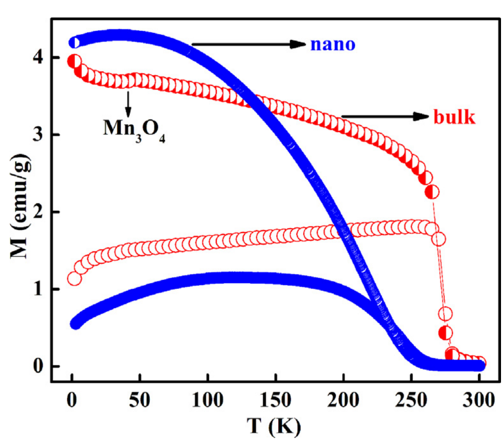

Fig. 4. Magnetization as a function of the temperature of bulk and nanocrystalline $Nd_{0.50}\square_{0.17}Sr_{0.33}MnO_3$ compounds.

abnormality of change in magnetization is may be due to the temperature dependence of the magnetic anisotropy of the nanocrystalline compound [56,57]. It is clear from the XAS data that more Mn^{3+} ions exist in the case of the nanocrystalline compound, the more Jahn-Teller distortions exist in the same. The Jahn-Teller effect has a direct dependence on the concentration of Mn^{3+} due to its double orbital degeneracy, and thus it has a strong interplay with DE interactions [14]. Thus the magnetic properties in the nanocrystalline compound are obviously due to the presence of more Jahn-Teller ions.

Further, to investigate this behavior, the hysteresis loop is measured for various temperature and is depicted in Fig. 5. The magnetization shows a sudden rise at lower magnetic field but does not show the level of saturation even at the higher magnetic field. Again, the magnetization of the nanocrystalline compound shows less value than that of its bulk counterpart at higher fields. It has been observed that the reduction of crystallite size has a strong influence on the magnetic and electric transport properties of nanocrystalline manganites. The observed results suggest that the nanocrystalline compound form like a core-shell structure, where the core is a ferromagnet while the shell behaves like a paramagnet [40]. As the grain size reduces, the surface-to-volume ratio increases and the contribution from the grain boundary effects increases. Thus the core of the nanocrystalline compound has physical properties the same as that of the bulk compound while the amorphous outer layer is magnetically disordered due to more oxygen vacancies and crystallographic defects [58]. Thus, due to the high disordered state in the outer shell, the net magnetic moment of this amorphous region becomes zero, which in turn reduces the magnetization. Since the shell behaves more like PM, the magnetization value of the nanocrystalline compound is lesser than its bulk counterparts. It is also noticed that the coercive field (H_C) decreases with the increase in temperature for both the compounds. As the magnetic anisotropy of the compound is proportional to the coercive field, it is evident that the crossover in magnetization is due to the sudden increase in the coercive field of the nanocrystalline compound while decreasing the temperature. There is a strong exchange coupling takes place between the inner core and outer shell of the nanocrystalline compound. The magnetically disordered state in the outer layer has a surface anisotropy contribution towards the effective anisotropy of the nanocrystalline compound [59]. The effect of the surface anisotropy increases with a decrease in crystallite size [59]. Thus the observed coercivity (one order higher) of the nanocrystalline compound is due to the surface anisotropy contribution by the insulating grain boundary growth.

In order to understand the broad ferromagnetic transition in the nanocrystalline compound, we have further carried out the temperature variation of AC susceptibility from 2 K to 300 K under frequencies from 333 Hz to 9984 Hz. Fig. 6(a) and (b) shows the in-phase and out of phase component of susceptibility, and it shows a maximum around T_C,

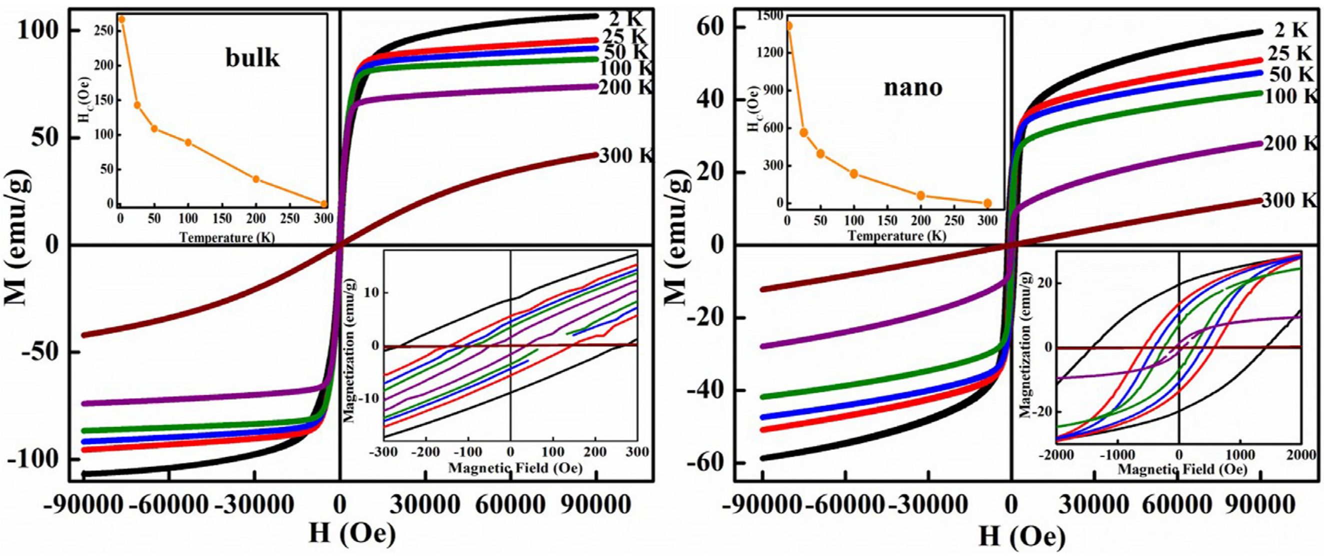

Fig. 5. Hysteresis loops of bulk and nanocrystalline $Nd_{0.50}\square_{0.17}Sr_{0.33}MnO_3$ compounds. The insets show the magnified view of the loop and temperature dependence of the coercive field.

and the obtained maximum is independent on the frequency change. The magnitude of the real part decreases and imaginary part increases with increasing frequency. The peak temperature is found to be constant with the variation of temperature and frequency. The imaginary part of the ac susceptibility exhibit a low-temperature hump like behavior around 46 K and this is due to the ordering of Mn_3O_4 secondary phase and which was not seen in the FC curve of dc magnetization in the nanocrystalline compound. It could be because the core is surrounded by a shell which is randomly oriented spins resulting in the suppression of Mn_3O_4 ordering.

Further to analyze the nature of T_C, isothermal magnetization measurement has done for every 4 K around the T_C and is shown in Fig. 7. The magnetization increases gradually at lower fields for both the compounds and the magnetization values of the nanocrystalline compound are much lesser than the bulk counterpart. The reduction of particle size in the nanocrystalline compound results in the suppression of magnetization due to the grain boundary effect [40]. The positive slope shown by the Arrott plot, a graph between M^2 and H/M confirms that the transition is second order in nature (shown in Fig. 7) [60]. We have also studied the magnetic entropy change (ΔS_M) of both the compounds using thermodynamic Maxwell relations [61]. Fig. 8 shows the ΔS_M for both the compounds estimated under 10 KOe and 50 KOe. The Bulk compound shows maximum values of 1.65 J kg^{-1} K^{-1} and 4.89 J kg^{-1} K^{-1} at 275 K for 10 kOe and 50 KOe respectively. However, the nanocrystalline compound shows a maximum value of 0.19 J kg^{-1} K^{-1} at 222 K and 0.98 J kg^{-1} K^{-1} at 226 K for fields of 10 kOe and 50 kOe respectively. The results obtained in the present study is comparable to numerous perovskite manganites and is given in Table 3. From the table it is clear that the bulk compound shows a significant ΔS_M and could be a potential candidate for magnetic refrigeration applications. It is observed that due to the domain boundary modification, the ΔS_M value of the nanocrystalline compound is lower than that of its bulk counterpart by one order.

The change in resistivity as a function of temperature, ρ(T) is shown in Fig. 9 and it is to be noted that the resistivity values of the nanocrystalline compound are found to be four orders higher than that of its bulk counterpart. Due to the grain boundary effect, the resistivity of the nanocrystalline compound increases. The mobility of the electrons decreases with an increase in crystallite size [59]. Due to the trapping of electrons at the grain boundary, a potential barrier is developed [59].

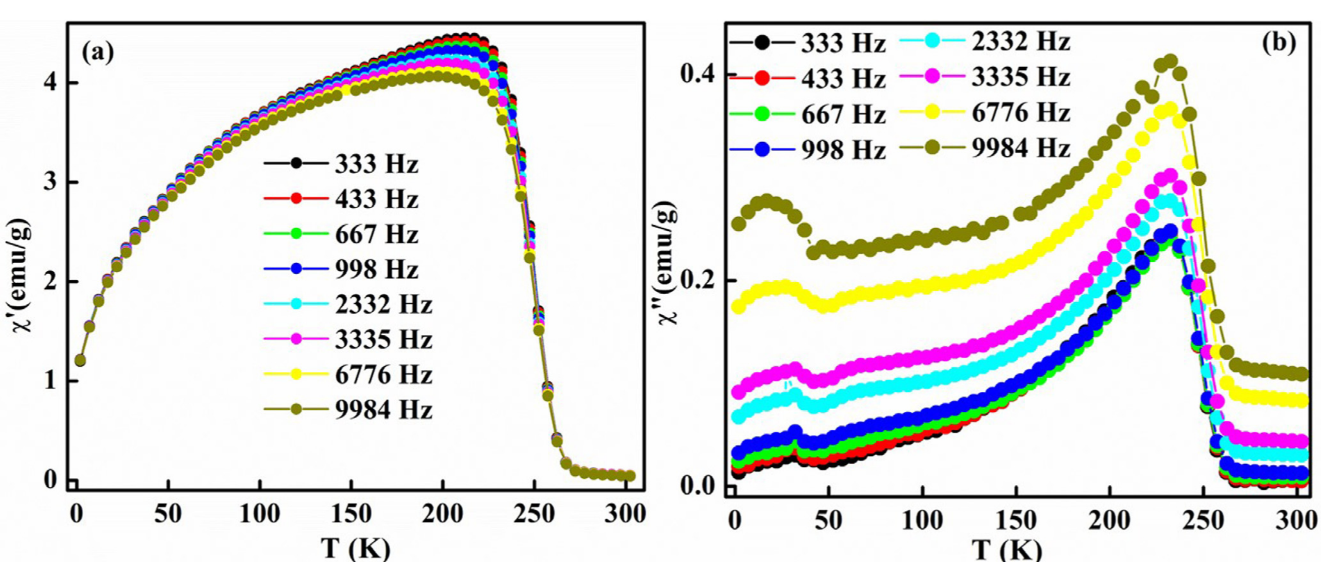

Fig.6. AC magnetic susceptibility of the nanocrystalline $Nd_{0.50}\square_{0.17}Sr_{0.33}MnO_3$ compound with real and imaginary parts.

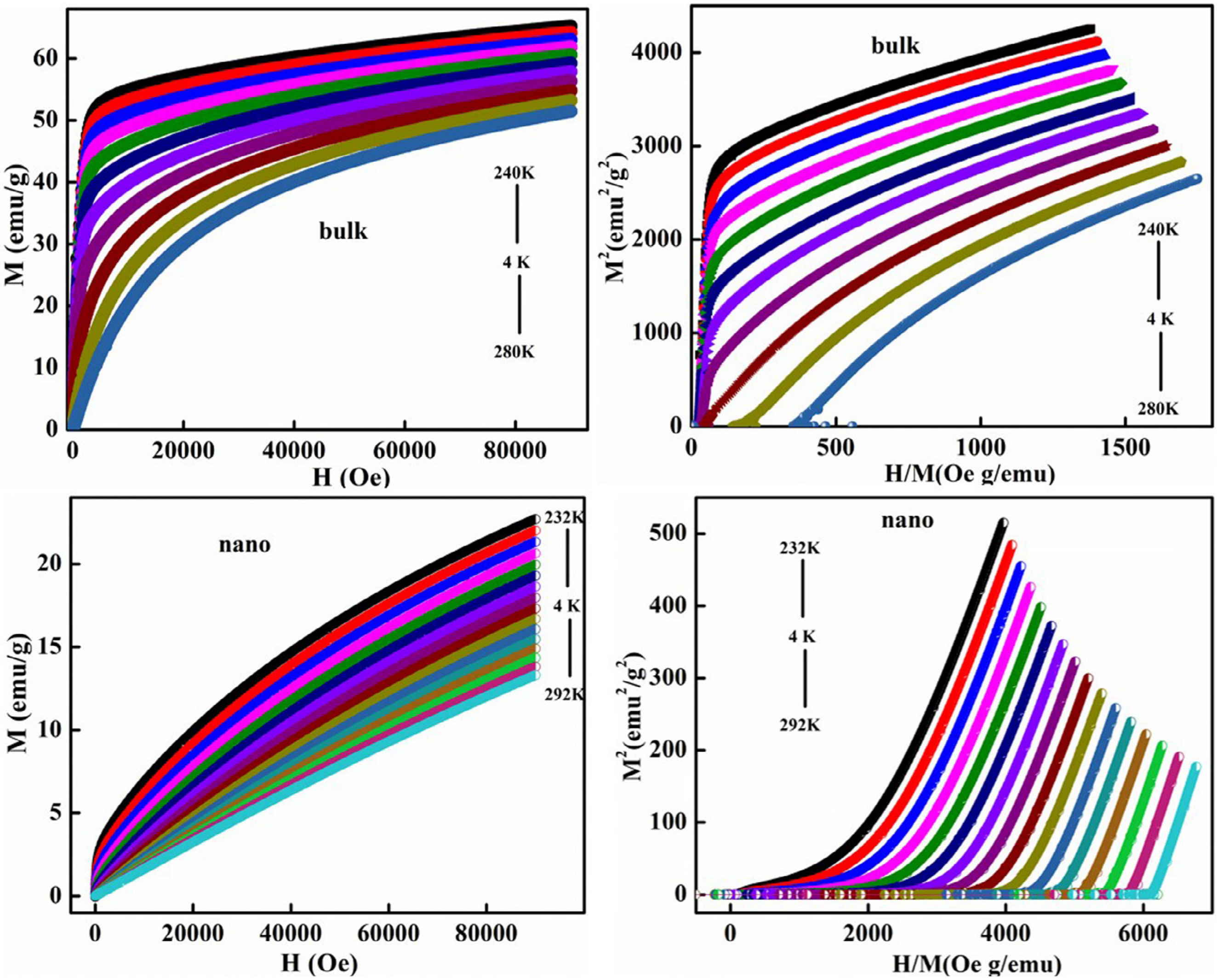

Fig. 7. M-H and Arrott plots of bulk and nanocrystalline $Nd_{0.50}\square_{0.17}Sr_{0.33}MnO_3$ compounds.

The e_g electrons in the outer shell are localized, and the interfacial layers are highly resistive to the electrons flow. Therefore a higher resistivity is observed with a decrease in crystallite size [59]. Thus the broken symmetry due to the grain surface effects has a strong influence on the electrical resistivity of nanocrystalline manganites. Both bulk and nanocrystalline compounds exhibit a sharp metal to insulator transition (say T_{P1}), near to the T_C. On further decreasing the temperature, the resistivity graph shows a broad maximum (say T_{P2}) below T_C and further it shows an upturn by making a low-temperature minimum (say T_m). The lacuna at the Nd-site creates trapped mobile electrons, which results in the coexistence of FM metallic (FMM) and FM insulating (FMI) phases [67]. The resistivity of the compound does not show a complete metallic character due to these coexisting phases. On further decreasing the temperature, the FMI phase decreases and the percolating path between FMM phases increases lead to a broad transition below T_C. In the nanocrystalline compound, T_{P2} is broader, and T_m is more prominent compared to its bulk counterparts. The double peak behavior with an abnormal point at 280 K in the bulk compound could be due to these electronic phase separation, and which is more prominent in the absence of magnetic fields. However, under high magnetic fields, the charge carriers delocalizes causing ordering of the magnetic spins results in shifting of peak to the higher temperatures. Thus with increasing magnetic fields, the abnormal point in the resistivity peak becomes weaken and disappear due to the complete transformation of the existing FMI phases into the FMM phases. The higher value of ρ(T) along with the metallic behavior in the FM region in the nanocrystalline compound can be understood due to the amorphous nature of grain boundary in the shell which is surrounded to the FM core. These results further corroborate the formation of core-shell type structure in case of the nanocrystalline compound. The magnetoresistance (MR) for different temperatures are calculated and shown in Fig. 9. The suppression of magnetic spin scattering takes place via local ordering for higher field, and the corresponding MR values also increase with field [68]. The bulk compound shows 50% of MR at 270 K, whereas the nanocrystalline compound shows 42% MR at 230 K for 90 kOe magnetic field.

To further understand the contribution of different parameters causing the conduction mechanism at low temperature ($T < T_P$), we have fitted the ρ(T) data of bulk compound using different theoretical models. The squared linear correlation coefficients are compared for each relation and Eq. (3) is obtained for the best fit for the experimental data

$$\rho = \rho_0 + \rho_2 T^2 + \rho_p T^5 + \rho_{4.5} T^{4.5}, \tag{3}$$

where $\rho_{0,}$ $\rho_2 T^{\ 2}$, $\rho_P\ T^5$ and $\rho_{4.5}T^{4.5}$ are the contribution from the grain boundary, electron-electron, phonon, and electron– magnon scattering processes respectively [69–72]. The best fit obtained using Eq. (3) for the bulk compound is shown in Fig. 10 (a), and fitted parameters are shown in Table 4. However, the nanocrystalline compound did not obey Eq. (3) because it could not explain the minima at the low-temperature

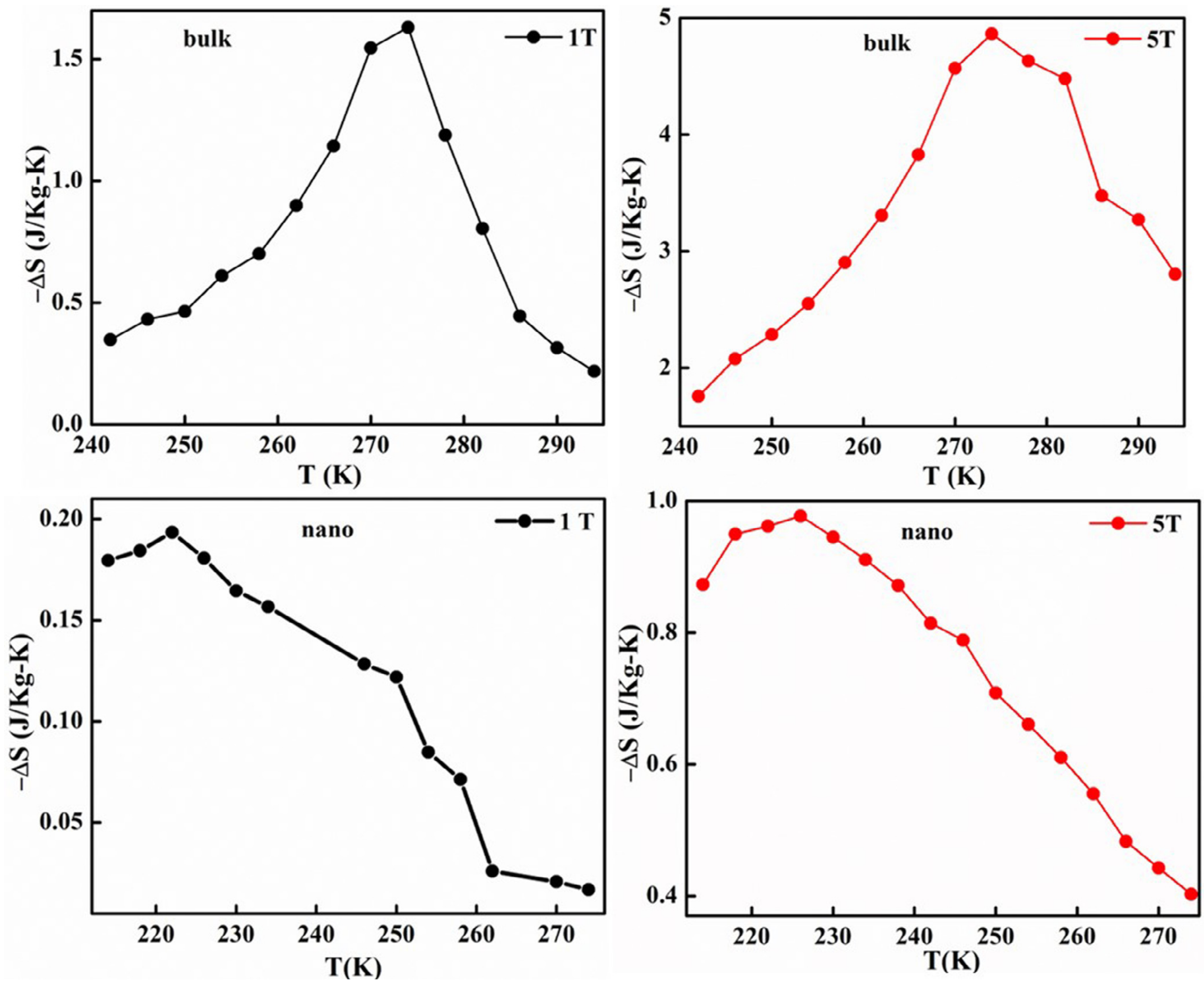

Fig. 8. The magnetic entropy change of bulk and nanocrystalline $Nd_{0.50}\square_{0.17}Sr_{0.33}MnO_3$ compounds.

region. The low-temperature resistivity minima in the nanocrystalline compound are sensitive to the magnetic fields and the shifting of it towards low temperature with the field. Again, the resistivity value of the nanocrystalline compound is found to increase after T_m, and the compound behaves like an insulator. Thus instead of showing metallic character in the ferromagnetic region, the nanocrystalline compound exhibits an anomalous behavior of insulating nature. It has been reported that the resistivity minima is a direct evidence for the Kondo-like

Table 3
Comparison of magnetocaloric properties of bulk and nanocrystalline $Nd_{0.50}\square_{0.17}Sr_{0.33}MnO_3$ compounds with several magnetocaloric materials.

Composition	Type of material	ΔH(kOe)	T_C (K)	ΔS_M (J kg^{-1} K^{-1})	Reference
$La_{0.67}Sr_{0.33}MnO_3$	Film	50	348	1.69	[62]
$La_{0.7}Sr_{0.25}\square_{0.05}MnO_3$	Nanocrystalline	50	328	1.33	[48]
$La_{0.65}Ba_{0.15}\square_{0.2}MnO_3$	Bulk	50	288	4.12	[49]
$La_{0.6}Ca_{0.15}\square_{0.05}Ba_{0.2}$ MnO_3	Bulk	50	202	2.69	[63]
$La_{0.6}Ca_{0.2}Ba_{0.15}\square_{0.05}$ MnO_3	Bulk	50	295	2.84	[63]
$La_{0.8}\square_{0.2}MnO_3$	Nanocrystalline	50	275	4.54	[64]
$La_{0.8}Na_{0.05}\square_{0.15}MnO_3$	Bulk	50	260	6.32	[28]
$Nd_{0.67}Sr_{0.33}MnO_3$	Bulk	10	232	2.69	[40]
$Nd_{0.67}Sr_{0.33}MnO_3$	Nanocrystalline	10	66	1.61	[40]
$Nd_{0.63}Sr_{0.37}MnO_3$	Single crystal	50	300	8.52	[65]
$Pr_{0.52}Sr_{0.48}MnO_3$	Single crystal	50	275	3.38	[66]
$Pr_{0.6}\square_{0.2}Sr_{0.2}MnO_3$	Nanocrystalline	50	276	1.50	[29]
$Pr_{0.53}\square_{0.17}Sr_{0.3}MnO_3$	Nanocrystalline	50	286	1.53	[29]
$(RE_{MIX})_{0.67}Sr_{0.33}MnO_3$	Bulk	10	310	1.01	[21]
$Nd_{0.50}\square_{0.17}Sr_{0.33}MnO_3$	Bulk	10	275	1.65	present work
$Nd_{0.50}\square_{0.17}Sr_{0.33}MnO_3$	Bulk	50	275	4.89	present work
$Nd_{0.50}\square_{0.17}Sr_{0.33}MnO_3$	Nanocrystalline	10	222	0.19	present work
$Nd_{0.50}\square_{0.17}Sr_{0.33}MnO_3$	Nanocrystalline	50	226	0.98	present work

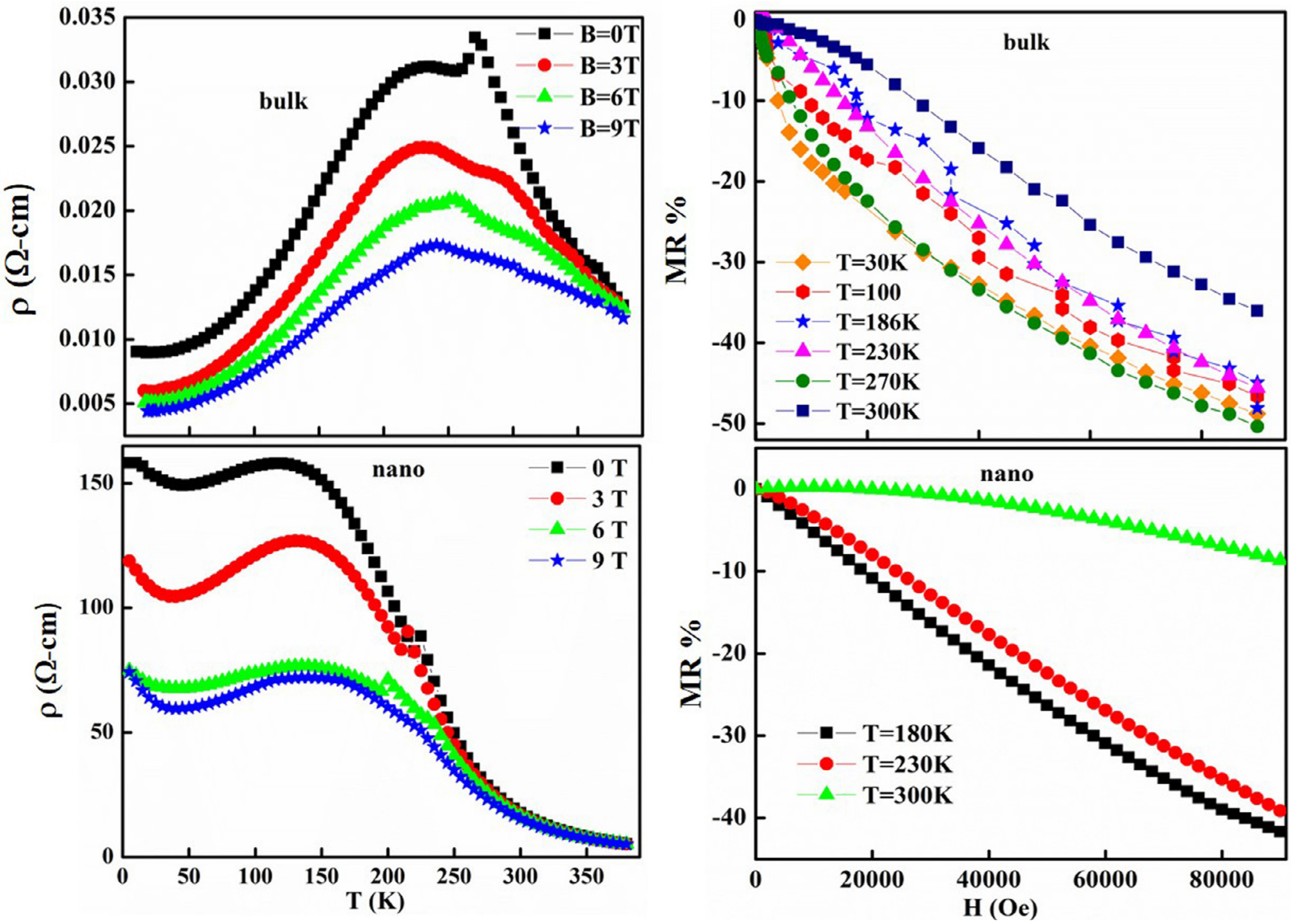

Fig. 9. Electrical transport behavior and magnetoresistance as a function of field of bulk and nanocrystalline $Nd_{0.50}\square_{0.17}Sr_{0.33}MnO_3$ compounds.

spin-dependent scattering mechanism and it is generally found in metals, materials with a small amount of magnetic impurities and also in manganites [73,74]. Thus the anomalous behavior of resistivity minima in the ferromagnetic region might have originated from the Kondo effect and strongly correlated effect in addition to all the parameters mentioned in Eq. (3). Thus we have obtained the best fitting, i.e., Eq. (4) for the nanocrystalline compound by modifying Eq. (3) with two additional parameters as

$$\rho = \rho_0 + \rho_e T^{1/2} -{-}\rho_s \ln T + \rho_2 T^2 + \rho_P T^5 + \rho_{4.5} T^{4.5} \tag{4}$$

where $\rho_s \ln T$ and $T^{1/2}$ are due to Kondo-like spin-dependent scattering and strongly correlated effect (electron-electron interactions) respectively [52,72–74]. The best fit obtained for the nanocrystalline compound is shown in Fig. 11 and fitted parameters are shown in Table 4.

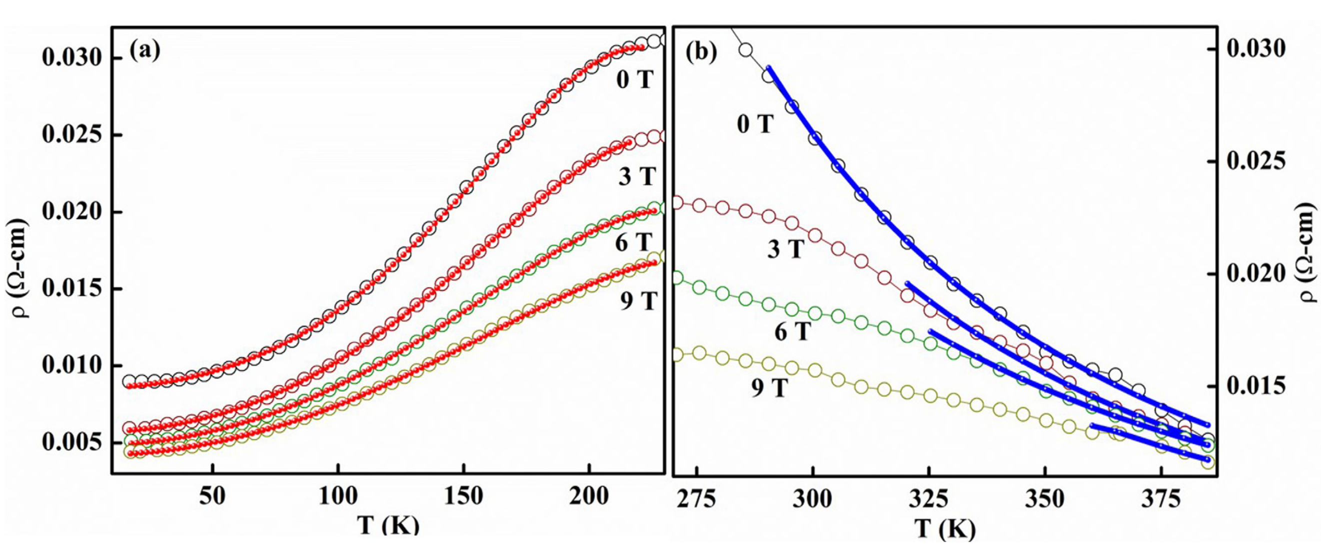

Fig. 10. Electrical resistivity as a function of the temperature of bulk $Nd_{0.50}\square_{0.17}Sr_{0.33}MnO_3$ compound along with the fittings to the Eqs. (3) and (5).

Table 4
Fitted parameters obtained for the best fit for both the compounds.

	Bulk-Low Temperature				High Temperature	
H (T)	$\rho_0 \times 10^{-5}$ (Ω m)	$\rho_2 \times 10^{-9}$ (Ω m/K^2)	$\rho_P \times 10^{-15}$ (Ω m/K^5)	$\rho_{4.5} \times 10^{-14}$ (Ω m/K$^{4.5}$)	B × 10^{-8} (Ω m)	E_a/K_B (K)
0	8.550	4.079	1.941	2.948	1.289	1265.12
3	5.680	4.189	1.021	1.478	1.452	1198.06
6	4.850	3.703	0.546	0.726	1.995	1070.66
9	4.200	3.254	0.214	0.217	1.759	1098.27

	Nanocrystalline-Low Temperature						High Temperature	
H (T)	ρ_0 (Ω m)	$\rho_2 \times 10^{-5}$ (Ω m/K^2)	$\rho_P \times 10^{-11}$ (Ω m/K^5)	$\rho_{4.5} \times 10^{-10}$ (Ω m/K$^{4.5}$)	$\rho_e \times 10^{-1}$(Ω (Ω m/K$^{1/2}$)	ρ_s (Ω m)	B × 10^{-6} (Ω m)	E_a/K_B (K)
0	1.607	9.280	5.753	8.951	1.576	0.202	1.133	1863.94
3	1.310	8.180	3.126	5.521	0.902	0.049	1.579	1743.62
6	0.814	3.060	1.088	1.949	0.303	0.018	3.776	1514.88
9	0.864	6.664	3.988	6.193	0.770	0.032	10.058	1227.64

The temperature dependence of resistivity above the metal-insulator transition is explained on the basis of small polaron hopping (SPH) mechanism [75]. In the adiabatic SPH model, ρ is expressed as

$$\rho = BT\exp(E_a/k_BT) \tag{5}$$

where B and E_a are the coefficient of resistivity and activation energy respectively. The graph (not shown) between ln (ρ/T) and 1/T has followed a linear relation indicates that the SPH model has dominated the electrical resistivity at the high-temperature region. We have fitted the variation of resistivity at high temperature using Eq. (5) for bulk and nanocrystalline compounds and shown in Figs. 10(b) and 11 respectively. Using the fittings to the Eq. (5), we have calculated the values of B and E_a for both the compounds and the results are shown in Table 4. The ρ(T) data analysis suggests that the conduction mechanism at higher temperatures takes place via adiabatic small polaron hopping whereas low-temperature conduction mechanism takes place because

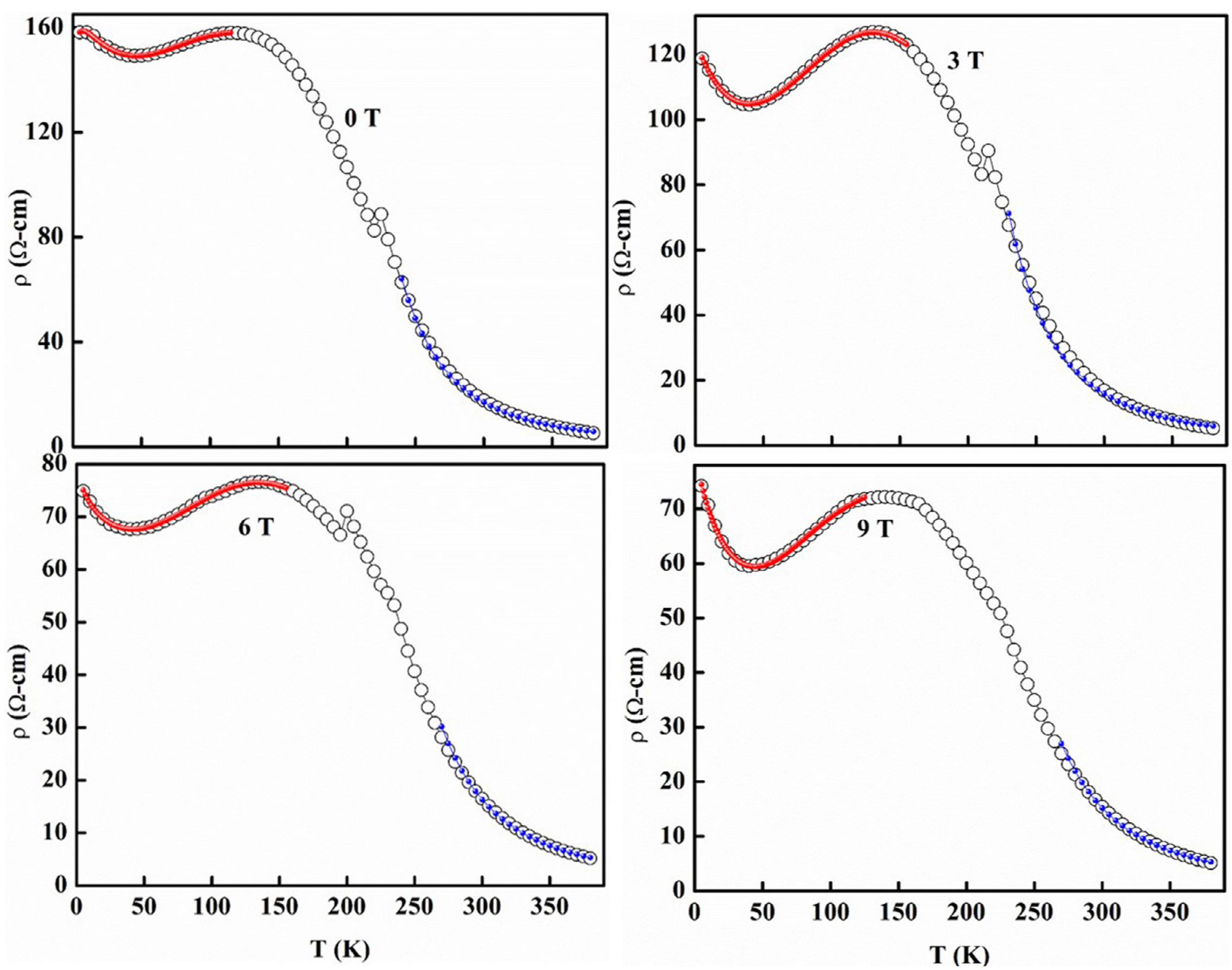

Fig. 11. Electrical resistivity as a function of the temperature of nanocrystalline $Nd_{0.50}\square_{0.17}Sr_{0.33}MnO_3$ compound along with the fittings to the Eqs. (4) and (5).

of the combined effects of grain boundaries, point-defect scattering electron-electron scattering, phonon scattering and electron-magnon scattering processes for both the compounds. In addition to that, in the case of the nanocrystalline compound, the Kondo effect and strong electron-electron interactions also play a vital role in the low-temperature conduction process.

4. Conclusion

The systematic investigation on the structural, magnetic and electrical transport properties of Nd-lacunar manganites are conducted. Orthorhombic crystal symmetry with Pbnm space group is confirmed from the Rietveld refinement, and morphological characterizations are done using SEM and TEM analysis. XAS analysis confirmed that the crystal field splitting energy is slightly higher for the nanocrystalline compound due to the broken symmetry at the surface. Both the bulk and nanocrystalline compounds show an enhancement in the magnetic transition temperature than that of its respective stoichiometric $Nd_{0.67}Sr_{0.33}MnO_3$ compound reported earlier. Temperature dependence of electrical resistivity under different magnetic fields show double peaks at higher temperatures, and an upturn at low-temperature and the latter is more prominent in the nanocrystalline compound. Kondo like spin-dependent scattering with electron-electron interactions dominates the low-temperature electrical transport behavior of the nanocrystalline compound, and small polaron hopping mechanism dominates at high temperatures for both the compounds. Further, enhancement in resistivity value of nanocrystalline compound suggests amorphous layers on the surface of FM core. The results revealed that the introduction of deficiency and crystallite size has a significant effect on the structural, magnetic and electrical transport properties of the studied compounds.

Acknowledgements

The authors would like to acknowledge the financial support received from the Department of Science and Technology sponsored project number, GAP232339. B. Arun and V.R. Akshay are thankful to Council of Scientific and Industrial Research, Government of India for granting the Senior Research Fellowship and also thankful to Academy of Scientific and Innovative Research, CSIR. The authors also thank the Board of Research in Nuclear Sciences, sponsored project no. GAP 218939 for partially supporting this work.

Appendix A. Supplementary data

Supplementary data to this article can be found online at https://doi.org/10.1016/j.jmmm.2018.09.124.

References

[1] S. Jin, M. McCormack, T.H. Tiefel, R. Ramesh, Colossal magnetoresistance in LaCaMnO ferromagnetic thin films, J. Appl. Phys. 76 (1994) 6929–6933.
[2] X.X. Zhang, J. Tejada, Y. Xin, G.F. Sun, K.W. Wong, X. Bohigas, Magnetocaloric effect in $La_{0.67}Ca_{0.33}MnO_\delta$ and $La_{0.60}Y_{0.07}Ca_{0.33}MnO_\delta$ bulk materials, Appl. Phys. Lett. 69 (1996) 3596–3598.
[3] B. Raveau, A. Maignan, C. Martin, M. Hervieu, Colossal magnetoresistance manganite perovskites: relations between crystal chemistry and properties, Chem. Mater. 10 (1998) 2641–2652.
[4] X. Bohigas, J. Tejada, E. del Barco, X.X. Zhang, M. Sales, Tunable magnetocaloric effect in ceramic perovskites, Appl. Phys. Lett. 73 (1998) 390–392.
[5] J.M.D. Coey, M. Viret, S. von Molnar, Mixed-valence manganites, Adv. Phys. 48 (1999) 167–213.
[6] M.B. Salamon, M. Jaime, The physics of manganites: structure and transport, Rev. Mod. Phys. 73 (2001) 583–628.
[7] C. Moure, O. Pena, Magnetic features in $REMeO_3$ perovskites and their solid solutions (RE = rare-earth, Me = Mn, Cr), J. Magn. Magn. Mater. 337–338 (2013) 1–22.
[8] C. Zener, Interaction between the d-Shells in the Transition Metals. II. Ferromagnetic compounds of manganese with perovskite structure, Phys. Rev. 82 (1951) 403–405.
[9] R. Cortes-Gil, L. Ruiz-Gonzalez, J.M. Alonso, M. Garcia-Hernandez, A. Hernando, J.M. Gonzalez-Calbet, Stair-like metamagnetic transition induced by controlled introduction of oxygen deficiency in $La_{0.5}Ca_{0.5}MnO_{3-\delta}$, Chem. Mater. 24 (2012) 2519–2526.
[10] E. Dixon, J. Hadermann, M.A. Hayward, Structures and magnetism of $La_{1-x}Sr_xMnO_{3-(0.5+x)/2}$ ($0.67 \leq x \leq 1$) Phases, Chem. Mater. 24 (2012) 1486–1495.
[11] Y. Sun, X. Xu, Y. Zhang, Large magnetic entropy change in the colossal magnetoresistance material $La_{2/3}Ca_{1/3}MnO_3$, J. Magn. Magn. Mater. 219 (2000) 183–185.
[12] L. Malavasi, C. Ritter, M.C. Mozzati, C. Tealdi, M.S. Islam, C.B. Azzoni, G. Flor, Effects of cation vacancy distribution in doped $LaMnO_{3+\delta}$ perovskites, J. Solid State Chem. 178 (2005) 2042–2049.
[13] F. Damay, C. Martin, A. Maignan, M. Hervieu, B. Raveau, Z. Jirak, G. Andre, F. Bouree, Magnetic and structural transitions in the half-doped manganites $Pr_{0.5}Sr_{0.5-x}Ca_xMnO_3$, Chem. Mater. 11 (1999) 536–541.
[14] A.J. Millis, B.I. Shraiman, R. Muller, Dynamic jahn-teller effect and colossal magnetoresistance in $La_{1-x}Sr_xMnO_3$, Phys. Rev. Lett. 77 (1996) 175–178.
[15] R. Epherre, C. Pepin, N. Penin, E. Duguet, S. Mornet, E. Pollert, G. Goglio, Evidence of non-stoichiometry effects in nanometric manganite perovskites: influence on the magnetic ordering temperature, J. Mater. Chem. 21 (2011) 14990–14998.
[16] P.M. Woodward, D.E. Cox, T. Vogt, C.N.R. Rao, A.K. Cheetham, Effect of compositional fluctuations on the phase transitions in $(Nd_{1/2}Sr_{1/2})MnO_3$, Chem. Mater. 11 (1999) 3528–3538.
[17] B.S. Nagaraja, A. Rao, G.S. Okram, Structural, electrical, magnetic and thermal studies on $Eu_{1-x}Sr_xMnO_3$ ($0.2 \leq x \leq 0.5$) manganites, J. Alloy. Compd. 683 (2016) 308–317.
[18] G. Venkataiah, P.V. Reddy, Electrical behavior of sol-gel prepared $Nd_{0.67}Sr_{0.33}MnO_3$ manganite system, J. Magn. Magn. Mater. 285 (2005) 343–352.
[19] D.C. Krishna, Y.K. Lakshmi, B. Sreedhar, P.V. Reddy, Magnetic transport behavior of nanocrystalline $Nd_{0.67}A_{0.33}MnO_3$ (A = Ca, Sr, Pb and Ba), Solid State Sci. 11 (2009) 1312–1318.
[20] Y.I. Chang, C.K. Ong, Iron-induced magnetic, transport and magnetoresistance behavior in $Nd_{0.67}Sr_{0.33}MnO_3$ epitaxial films, J. Appl. Phys. A 79 (2004) 2103–2107.
[21] B. Arun, V.R. Akshay, G.R. Mutta, C. Venkatesh, M. Vasundhara, Mixed rare earth oxides derived from monazite sand as an inexpensive precursor material for room temperature magnetic refrigeration applications, Mater. Res. Bull. 94 (2017) 537–543.
[22] A. Rostamnejadi, M. Venkatesan, P. Kameli, H. Salamati, J.M.D. Coey, Magnetocaloric effect in $La_{0.67}Sr_{0.33}MnO_3$ manganite above room temperature, J. Magn. Magn. Mater. 323 (2011) 2214–2218.
[23] W. Boujelben, A. Cheikh-Rouhou, J. Pierre, J.C. Joubert, Ferromagnetism in the lacunar (Pr, Sr)MnO_3perovskite manganites, Phys. B 321 (2002) 37–44.
[24] M. Ellouze, W. Boujelben, A. Cheikhrouhou, H. Fuess, R. Madar, Structure, magnetic and electrical properties in the praseodymium deficient $Pr_{0.8-x}\gamma_xSr_{0.2}MnO_3$ manganites oxides, J. Alloy. Compd. 325 (2003) 41–47.
[25] M. Khlifi, A. Tozri, M. Bejar, E. Dhahri, E.K. Hlil, Effect of calcium deficiency on the critical behavior near the paramagnetic to ferromagnetic phase transition temperature in $La_{0.8}Ca_{0.2}MnO_3$ oxides, J. Magn. Magn. Mater. 324 (2012) 2142–2146.
[26] R. Bellouz, M. Oumezzine, A. Dinia, G. Schmerber, E. Hlil, M. Oumezzine, Magnetocaloric properties of $La_{0.65}Eu_{0.05}Sr_{0.3-x}MnO_3$ ($0 \leq x \leq 0.15$) perovskites, RSC Adv. 5 (2015) 64557–64565.
[27] W. Cheikh-Rouhou Koubaa, M. Koubaa, A. Cheikh-Rouhou, W. Boujelben, A.M. Haghiri-Gosnet, A-site deficiency effects on the structure, magnetic and transport properties of $Pr_{0.6-x}\gamma_xSr_{0.4}MnO_3$ ($0 \leq x \leq 0.2$) perovskite manganite, J. Alloy. Compd. 455 (2008) 67–72.
[28] M. Wali, R. Skini, M. Khlifi, E. Dhahri, E.K. Hlil, A giant magnetocaloric effect with a tunable temperature transition close to room temperature in Na-deficient $La_{0.8}Na_{0.2-x}\gamma_xMnO_3$ manganites, Dalton Trans. 44 (2015) 12796–12803.
[29] B. Arun, M. Athira, V.R. Akshay, B. Sudakshina, G.R. Mutta, M. Vasundhara, Investigation on the structural, magnetic and magnetocaloric properties of nanocrystalline Pr-deficient $Pr_{1-x}Sr_xMnO_{3-\delta}$ manganites, J. Magn. Magn. Mater. 448 (2018) 322–331.
[30] L. Malavasi, Role of defect chemistry in the properties of perovskite manganites, J. Mater. Chem. 18 (2008) 3295–3308.
[31] F. Elleuch, M. Triki, M. Bekri, E. Dhahri, E.K. Hlil, A-site-deficiency-dependent structural, magnetic and magnetoresistance properties in the $Pr_{0.6}Sr_{0.4}MnO_3$ manganites, J. Alloy. Compd. 620 (2015) 249–255.
[32] A.E. Danks, S.R. Hall, Z. Schnepp, The evolution of 'sol-gel' chemistry as a technique for materials synthesis, Mater. Horiz. 3 (2016) 91–112.
[33] M. Pechini, Method of preparing lead and alkaline earth titanates and niobates and coating method using the same to form a capacitor, US Patent 97, 1967, 3306.
[34] S. Zhou, Y. Guo, J. Zhao, L. He, C. Wang, L. Shi, Particle size effects on charge and spin correlations in $Nd_{0.5}Ca_{0.5}MnO_3$ nanoparticles, J. Phys. Chem. C 115 (2011) 11500–11506.
[35] S. Zhou, Y. Guo, C. Wang, L. He, J. Zhao, L. Shi, Magnetic phase diagram of nanosized half-doped manganites: role of size reduction, Dalton Trans. 41 (2012) 7109–7114.
[36] T. Zhang, X.P. Wang, Q.F. Fang, Evolution of the electronic phase separation with magnetic field in bulk and nanometer $Pr_{0.67}Ca_{0.33}MnO_3$ particles, J. Phys. Chem. C 115 (2011) 19482–19487.
[37] N.D. Thorat, K.P. Shinde, S.H. Pawar, K.C. Barick, C.A. Betty, R.S. Ningthoujam, Polyvinyl alcohol: an efficient fuel for synthesis of superparamagnetic LSMO nanoparticles for biomedical application, Dalton Trans. 41 (2012) 3060–3071.
[38] A. Sadhu, T. Kramer, A. Datta, S.A. Wiedigen, J. Norpoth, C. Jooss, S. Bhattacharyya, Ferromagnetism in lightly doped $Pr_{1-x}Ca_xMnO_3$ (x = 0.023, 0.036) nanoparticles synthesized by microwave irradiation, Chem. Mater. 24 (2012) 3758–3764.

[39] A. Sadhu, S. Bhattacharyya, Enhanced low-field magnetoresistance in $La_{0.71}Sr_{0.29}MnO_3$ nanoparticles synthesized by the nonaqueous Sol – Gel Route, Chem. Mater. 26 (2014) 1702–1710.

[40] B. Arun, M.V. Suneesh, M. Vasundhara, Comparative study of magnetic ordering and electrical transport in bulk and nano-grained $Nd_{0.67}Sr_{0.33}MnO_3$ manganites, J. Magn. Magn. Mater. 418 (2016) 265–272.

[41] B. Sudakshina, B. Arun, K.D. Chandrasekhar, H.D. Yang, M. Vasundhara, Structural and magnetic properties of $Nd_{0.67}Ba_{0.33}MnO_3$ manganites with partial replacement of Fe and Cu at Mn-site, Phys. B Condens. Matter. 539 (2018) 14–20.

[42] C. Vazquez-Vazquez, M.C. Blanco, M.A. Lopez-Quintela, R.D. Sanchez, J. Rivas, S.B. Oseroff, Characterization of $La_{0.67}Ca_{0.33}MnO_{3\pm\delta}$ particles prepared by the sol-gel route, J. Mater. Chem. 8 (4) (1998) 991–1000.

[43] J. Spooren, R.I. Walton, F. Millange, A study of the manganites $La_{0.5}M_{0.5}MnO_3$ (M = Ca, Sr, Ba) prepared by hydrothermal synthesis, J. Mater. Chem. 15 (2005) 1542–1551.

[44] R. Skini, A. Omri, M. Khlifi, E. Dhahri, E.K. Hlil, Large magnetocaloric effect in lanthanum-deficiency manganites $La_{0.8-x}\square_xCa_{0.2}MnO_3$($0.00 \le x \le 0.20$) with a first-order magnetic phase transition, J. Magn. Magn. Mater. 364 (2014) 5–10.

[45] S. Hcini, S. Zemni, M. Boudard, H. Rahmouni, M. Oumezzine, Synthesis, structural, magnetic and electrical properties of nominal La0.67Ba0.33-xNaxMnO3 ($0 \le x \le 0.33$) manganites, EPJ Web of Conferences 29, 2012, 00022/1-10.

[46] A. Guinier, Theorie et Technique de la Radiocristallographie, Dunod, 1964.

[47] R. Skini, M. Khlifi, M. Jemmali, E. Dhahri, E.K. Hlil, Influence of disorder on the appearance of Griffiths phases in $La_{0.8-x}\square_xCa_{0.2}MnO_3$ (x = 0.15 and 0.2) compounds, Phys. B 457 (2015) 314–319.

[48] J. Makni-Chakroun, I. Sfifir, W. Cheikhrouhou-Koubaa, M. Koubaa, A. Cheikhrouhou, Structural, magnetic magnetocaloric effect and critical behavior of $La_{0.7}Sr_{0.3-xx}MnO_3$ ($0 \le x \le 0.05$), J. Magn. Magn. Mater. 432 (2017) 484–493.

[49] A. Marzouki-Ajmi, H. Omrani, W. Cheikhrouhou-Koubaa, M. Koubaa, A. Cheikhrouhou, Effect of barium-deficiency on the structural, magnetic, and magnetocaloric properties of $La_{0.65}Ba_{0.35-x}\square_xMnO_3$ ($0 \le x \le 0.2$) manganites, J. Alloy. Compd. 690 (2017) 403–411.

[50] M. Wali, R. Skini, M. Khlifi, E. Dhahri, E.K. Hlil, Effect of the oxygen deficiency on the physical properties of $La_{0.8}Na_{0.2}MnO_{3-\delta}$ oxides ($\delta = 0$ and 0.05), J. Magn. Magn. Mater. 394 (2015) 207–211.

[51] B. Arun, M.V. Suneesh, B. Sudakshina, V.R. Akshay, K.D. Chandrasekhar, M. Vasundhara, Effects of Mn site substitution on magnetic ordering and critical behavior in $Nd_{0.67}Sr_{0.33}MnO_3$manganite, J. Phys. Chem. Solids 123 (2018) 327–335.

[52] H. Terashita, J.C. Cezar, F.M. Ardito, L.F. Bufaiçal, E. Granado, Element-specific and bulk magnetism, electronic, and crystal structuresof $La_{0.70}Ca_{0.30}Mn_{1-x}Cr_xO_3$, Phys. Rev. B 85 (2012) 104401/1- 9.

[53] J. Suntivich, W.T. Hong, Y.L. Lee, J.M. Rondinelli, W. Yang, J.B. Goodenough, B. Dabrowski, J.W. Freeland, Y. Shao-Horn, Estimating hybridization of transition metal and oxygen states in perovskites from O K-edge X-ray absorption spectroscopy, J. Phys. Chem. C 118 (2014) 1856–1863.

[54] M. Abbate, F.M.F. de Groot, J.C. Fuggle, A. Fujimori, O. Strebel, F. Lopez, M. Domke, G. Kaindl, G.A. Sawatzky, M. Takano, Y. Takeda, H. Eisaki, S. Uchida, Controlled-valence properties of $La_{1-x}Sr_xFeO_3$ and $La_{1-x}Sr_xMnO_3$ studied by soft-x-ray absorption spectroscopy, Phys. Rev. B 46 (1992) 4511–4519.

[55] B. Sudakshina, K.D. Chandrasekhar, H.D. Yang, M. Vasundhara, Observation of complex magnetic behaviour in calcium doped neodymium manganites, J. Phys. D. Appl. Phys. 50 (2017) 065004/1-11..

[56] C. Antoniak, J. Lindner, M. Farle, Magnetic anisotropy and its temperature dependence in iron-rich Fe_xPt_{1-x} nanoparticles, Europhys. Lett. 70 (2005) 250–256.

[57] S.S. Rao, S.V. Bhat, Magnetization magnetotransport and electron magnetic resonance studies of nanoparticles and nanowires of Pr0.5Sr0.5MnO3, J. Phys. D: Appl. Phys. 42 (2009) 075004/1-13.

[58] P. Dey, T.K. Nath, P.K. Manna, S.M. Yusuf, Enhanced grain surface effect on magnetic properties of nanometric $La_{0.7}Ca_{0.3}MnO_3$ manganite: Evidence of surface spin freezing of manganite nanoparticles, J. Appl. Phys. 104 (2008) 103907/1-12.

[59] V. Dyakonov, A. Slawska-Waniewska, N. Nedelko, E. Zubov, V. Mikhaylov, K. Piotrowski, A. Szytula, S. Baran, W. Bazela, Z. Kravchenko, P. Aleshkevich, A. Pashchenko, K. Dyakonov, V. Varyukhin, H. Szymczak, Magnetic resonance and transport properties of nanopowder of $La_{0.7}Sr_{0.3}MnO_3$ manganites, J. Magn. Magn. Mater. 322 (2010) 3072–3079.

[60] B.K. Banerjee, On a generalized approach to first and second order magnetic transitions, Phys. Lett. 12 (1964) 16–17.

[61] M.H. Phan, S.B. Tian, S.C. Yu, A.N. Ulyanov, Magnetic and magnetocaloric properties of $La_{0.7}Ca_{0.3-x}Ba_xMnO_3$ compounds, J. Magn. Magn. Mater. 256 (2003) 306–310.

[62] D.T. Morelli, A.M. Mance, J.V. Mantese, A.L. Micheli, Magnetocaloric properties of doped lanthanum manganites films, J. Appl. Phys. 79 (1996) 373–375.

[63] I. Sfifir, H. Ben Khlifa, W. Cheikhrouhou-Koubaa, M. Koubaa, A. Cheikhrouhou, Vacancy effect in both calcium and barium on the physical properties of $La_{0.6}Ca_{0.2}Ba_{0.2}MnO_3$ polycrystalline manganite, J. Alloy. Compd. 693 (2017) 782–791.

[64] R. Skini, M. Khlifi, E.K. Hlil, Efficient composite magnetocaloric material with a tunable temperature transition in K-deficient manganites, RSC Adv. 6 (2016) 34271–34279.

[65] M.H. Phan, H.X. Peng, S.C. Yu, Large magnetocaloric effect in single crystal $Pr_{0.63}Sr_{0.37}MnO_3$, J. Appl. Phys. 97 (2005) 10M306/1-3.

[66] M. Patra, S. Majumdar, S. Giri, G.N. Iles, T. Chatterji, Anomalous magnetic field dependence of magnetocaloric effect at low temperature in $Pr_{0.52}Sr_{0.48}MnO_3$ single crystal, J. Appl. Phys. 107 (2010) 076101/1-3.

[67] M. Uehara, S. Mori, C.H. Chen, S.-W. Cheong, Percolative phase separation underlies colossal magnetoresistance in mixed-valent manganites, Nature 399 (1999) 560–563.

[68] B. Sudakshina, B. Arun, M. Vasundhara, Electrical magnetic, and magnetotransport behavior of inhomogeneous $Nd_{1-x}Ca_xMnO_3$ ($0.0 \le x \le 0.8$) manganites, J. Magn. Magn. Mater. 448 (2018) 250–256.

[69] A. Urushibara, Y. Moritomo, T. Arima, A. Asamitsu, G. Kido, Y. Tokura, Insulator-metal transition and giant magnetoresistance in $La_{1-x}Sr_xMnO_3$, Phys. Rev. B 51 (1995) 14103–14109.

[70] M. Viret, L. Ranno, J.M.D. Coey, Magnetic localization in mixed-valence manganites, Phys. Rev. B 55 (1997) 8067–8070.

[71] M. Khlifi, M. Bejar, E. Dhahri, P. Lachkar, E.K. Hlil, Influence of Ca-deficiency on the magneto-transport properties in $La_{0.8}Ca_{0.2}MnO_3$ perovskite and estimation of magnetic entropy change, J. Appl. Phys. 111 (2012) 103909/1-6.

[72] G. Lalitha, P.V. Reddy, Low- temperature resistivity anomalies and magnetic field-induced transitions in neodymium-based manganites, Phys. Scr. 82 (2010) 045704/1-10.

[73] J. Kondo, Resistance minimum in dilute magnetic alloys, Prog. Theor. Phys. 32 (1964) 37–49.

[74] J. Zhang, Y. Xu, S. Cao, G. Cao, Y. Zhang, C. Jing, Kondo-like transport and its correlation with the spin-glass phase in perovskite manganites, Phys. Rev. B 72 (2005) 054410/1-6.

[75] A. De Andres, M. Garcıa-Hernández, J.L. Martınez, C. Prieto, Low-temperature magnetoresistance in polycrystalline manganites: connectivity versus grain size, Appl. Phys. Lett. 74 (1999) 3884–3886.